Preparation, characterization and photocatalytic activity of nano-sized ZnO/SnO$_2$ coupled photocatalysts

Wang Cun [a],[*], Zhao Jincai [b], Wang Xinming [a], Mai Bixian [a],
Sheng Guoying [a], Peng Ping'an [a], Fu Jiamo [a]

[a] *Guangzhou Institute of Geochemistry, Chinese Academy of Sciences, Guangzhou 510640, PR China*
[b] *Institute of Chemistry, Chinese Academy of Sciences, Beijing 100080, PR China*

Abstract

The nano-sized coupled oxides ZnO/SnO$_2$ in a molar ratio of 2:1 (Z$_2$S) and 1:1 (ZS) were prepared using the co-precipitation method and characterized with X-ray diffraction (XRD), UV–VIS diffuse reflectance spectroscopy and specific surface area (Brunauer–Emmett–Teller (BET)). Their photocatalytic activities were also evaluated using methyl orange (MO) as a model organic compound. The isothermal adsorption behavior of MO on Z$_2$S and the factors affecting the photocatalytic activity, such as the heat-treating temperature for the photocatalyst, the pH value of the reaction suspension and the addition of NaCl, KNO$_3$ and K$_2$SO$_4$ into the suspension, have been studied. It is found that the change in phase of Z$_2$S occurs with the calcination temperature. The band gap energy value observed by UV–VIS diffuse reflectance spectroscopy is 3.15 eV for Z$_2$S compared with those of 3.12 eV for ZS, 3.17 eV for ZnO and 2.53 eV for SnO$_2$. The isothermal adsorption behavior is a two-stage process. The photocatalytic degradation rate of MO on Z$_2$S is faster than that on ZS and ZnO by 40.2 and 66.1%, respectively. A schematic diagram of photocatalytic activity is also presented to explain the results.
© 2002 Elsevier Science B.V. All rights reserved.

Keywords: Photocatalyst; Zinc oxide; Tin oxide; Coupled nano-crystalline; Water purification; Methyl orange

1. Introduction

The degradation of organic pollutants in water and air by photocatalysis, using semiconductors, such as TiO$_2$ and ZnO, has attracted extensive attention during recent 20 years [1]. Previous studies have proved that such semiconductors can degrade most kinds of persistent organic pollutants, such as detergents, dyes, pesticides and volatile organic compounds, under UV-light irradiation [1–5]. However, the fast recombination rate of photogenerated electron/hole pairs hinders the commercialization of this technology [1]. It is of great interest to improve the photocatalytic activity of semiconductors for the degradation of organic compounds in water and air. In the past several years, there are a number of studies related to the photocatalytic activity of TiO$_2$ or ZnO coupled with metal oxide, like SnO$_2$ [6–11], WO$_3$ [12–16], Fe$_2$O$_3$ [17,18], ZrO$_2$ [19] and some rare earth oxides [20,21], for the purpose of improving TiO$_2$ or ZnO photocatalytic activity. Coupled semiconductor photocatalysts may increase the photocatalytic efficiency by increas-

* Corresponding author. Tel.: +86-20-85290180;
fax: +86-20-85290706.
E-mail address: wangcun@gig.ac.cn (W. Cun).

ing the charge separation and extending the energy range of photoexcitation. At the same time, their physical and optical properties are greatly modified [16].

Recently, Tennakone and Bandara demonstrated that, when SnO_2 nano-crystallites ($\sim$ 10–15 nm) are ground with ZnO powders ($\sim$ 600 nm) in the ZnO content of 54 and 40% by weight, respectively, the coupled oxide catalysts ZnO/SnO_2 can generate hydrogen from water in the presence of a sensitizer (ruthenium bipyridyl complex) and a hole scavenger (i.e. ethanol) under visible light irradiation [6]. These results can be explained as originating from the transfer of energetic electrons ('hot electrons') injected to SnO_2 via dye-sensitization to ZnO, whose conduction band (CB) position is above that of SnO_2, leading to a wide separation of the electron and the hole.

The photocatalytic activity of coupled oxide photocatalyst is closely related to the ratio of the two oxides [15,19]. The aim of the present study is to study the photocatalytic activity of Z_2S and ZS, which can be explained by a scheme illustrating the photocatalytic activity. For this purpose, the nano-sized coupled oxides Z_2S and ZS were prepared and their photocatalytic activities were evaluated using MO [22] as a model organic compound. The adsorption behavior of MO on Z_2S and the factors affecting the photocatalytic activity, such as the heat-treating temperature for Z_2S, the pH value of the reaction suspension as well as the concentration of NaCl, KNO_3 and K_2SO_4 in the suspension, have also been examined. It is found that the coupled oxide photocatalyst Z_2S has better photocatalytic activity to MO than ZS and ZnO.

2. Experimental

2.1. Preparation for nano-sized photocatalysts

Nano-sized coupled oxide photocatalyst Z_2S was prepared with the co-precipitation method. $SnCl_4 \cdot 5H_2O$ and $ZnSO_4 \cdot 7H_2O$ (analytic reagent grade) were used as the starting materials and NaOH as the co-precipitant without further purification. $ZnSO_4 \cdot 7H_2O$ and $SnCl_4 \cdot 5H_2O$ in a molar ratio of 2:1 were dissolved in a minimum amount of deionized water.

Then the 4 mol/l of NaOH solution was added to the above solution to adjust pH to about 7 and a white amorphous precipitate was formed. The precipitate was filtered and washed with deionized water till no SO_4^{2-} and Cl^- were found in filtrate. Then the wet powder was dried at about 100 °C in air to form the precursor of Z_2S. Finally, the precursor was calcined in air at a certain temperature to produce the nano-sized Z_2S photocatalysts. The nano-sized ZS, ZnO and SnO_2 were prepared in the same procedure as mentioned above except that the starting materials are $ZnSO_4 \cdot 7H_2O$ and $SnCl_4 \cdot 5H_2O$ in a molar ratio of 1:1 for ZS, $ZnSO_4 \cdot 7H_2O$ for ZnO and $SnCl_4 \cdot 5H_2O$ for SnO_2, respectively.

2.2. Characterizing Z_2S and ZS

To determine the crystal phase composition of the prepared photocatalysts, X-ray diffraction (XRD) measurement was carried out at room temperature by using a Rigaku D/max –1200 diffractometer with Cu Kα radiation ($\lambda = 0.15418$ nm). The accelerating voltage of 40 kV, emission current of 30 mA and the scanning speed of 4°/min were used. To determine the band gap energy of the photocatalysts, UV–VIS diffuse reflectance spectroscopy measurement was carried out using a Hitachi U-3010 (Japan) spectrophotometer with an integrating sphere. The pure powdered $BaSO_4$ was used as a reference sample. To determine the specific surface area of the photocatalysts, gas sorption analysis (Brunauer–Emmett–Teller (BET) method) was carried out by using a Quantachrome NOVA/1000 gas analyzer.

2.3. Adsorption behavior of MO on Z_2S

To determine the adsorption behavior of MO on Z_2S surface, the suspensions were prepared by mixing 10 ml aliquots of MO solutions of various initial concentrations (from 0 to 600 mg/l) at the natural pH value with a given weight (0.050 g) of Z_2S. The suspensions were kept overnight in the dark and filtered after being centrifuged. The absorbance of the filtrate was then measured at the maximum band 464 nm of MO to determine the concentration of MO. The extent of equilibrium adsorption was determined from the decrease in the MO concentration detected after

filtration. All the isotherm measurements were made in the dark.

2.4. Photocatalytic experiments

Photocatalytic experiments were conducted using photocatalysts to photocatalytically degrade MO in water solution. The MO is AR grade and used as supplied. The photocatalytic reactor consists of two parts: a 100 ml Pyrex glass bottle and a 300 W high pressure Hg lamp with a maximum emission at about 365 nm, which was positioned parallel to the Pyrex glass bottle. In all experiments, the reaction temperature was kept at $25 \pm 2\,^{\circ}\text{C}$ by using an air-conditioner.

Reaction suspensions were prepared by adding photocatalyst powders into a 100 ml of aqueous MO solutions. Prior to irradiation, the suspension was ultrasonically sonicated for 15 min and then magnetically stirred in a dark condition for 30 min to establish an adsorption/desorption equilibrium. The suspensions containing MO and photocatalyst were then irradiated under the UV light.

At given time intervals, analytical samples were taken from the reaction suspension and centrifuged at 9000 rpm for 10 min, filtered through a 0.2 μm millipore filter to remove the particles and the filtrate was then analyzed.

2.5. Analytical methods

MO concentration was analyzed by UV–VIS spectroscopy (Thermo Spectronic/Heλios α) at its maximum absorption wavelength of 464 nm. Total organic carbon (TOC) was determined by Dohrmann/Phoenix 8000/UV-persulfate TOC analyzer.

3. Results and discussions

3.1. Phase and mean size of the photocatalysts

The XRD patterns of the Z_2S powders calcined at different temperatures and for different times are as shown in Fig. 1(1) and (2), respectively. The phases of the photocatalysts calcined at 500 and 600 °C are the mixture of ZnO and SnO_2, but the grain sizes get larger with the increasing calcination temperature. The Zn_2SnO_4 phase emerges at 700 °C and ZnO and SnO_2 almost disappear at 900 °C. For the coupled oxide calcined at a fixed temperature of 600 °C, Fig. 1(2) shows that there are no changes in phase of the coupled oxide except that the diffraction peaks are continuously getting sharper, which reveals the mean sizes of the coupled oxide increase with calcination time. The mean sizes of the Z_2S calcined at 600 °C for 2, 6, 10 h and at 500, 700, 800 and 900 °C for 10 h, respectively, can be determined by Scherrer formula [23]. The phases and the mean sizes are listed in Table 1.

The phases of the ZS samples calcined at 500 and 600 °C, respectively, for 10 h are Zn_2SnO_4 and SnO_2 and no ZnO is found, which is different from the Z_2S calcined under the identical condition. The temperature for Zn_2SnO_4 formation in ZS is about 200 °C, lower than that in Z_2S, which means that excessive SnO_2 is favorable for ZnO and SnO_2 to form Zn_2SnO_4. The mean sizes of Zn_2SnO_4 and SnO_2 in ZS calcined at 600 °C for 10 h are about 17.6 and 5.3 nm, respectively.

The mean sizes of pure SnO_2 and ZnO calcined at 600 °C for 10 h are about 13.5 and 88.6 nm, respectively. This is another evidence that ZnO calcines more easily and, thus, tends to have larger grain size than SnO_2 [24]. An interesting phenomenon can be seen

Table 1
Dependence of phase and mean sizes of Z_2S on heat-treating condition

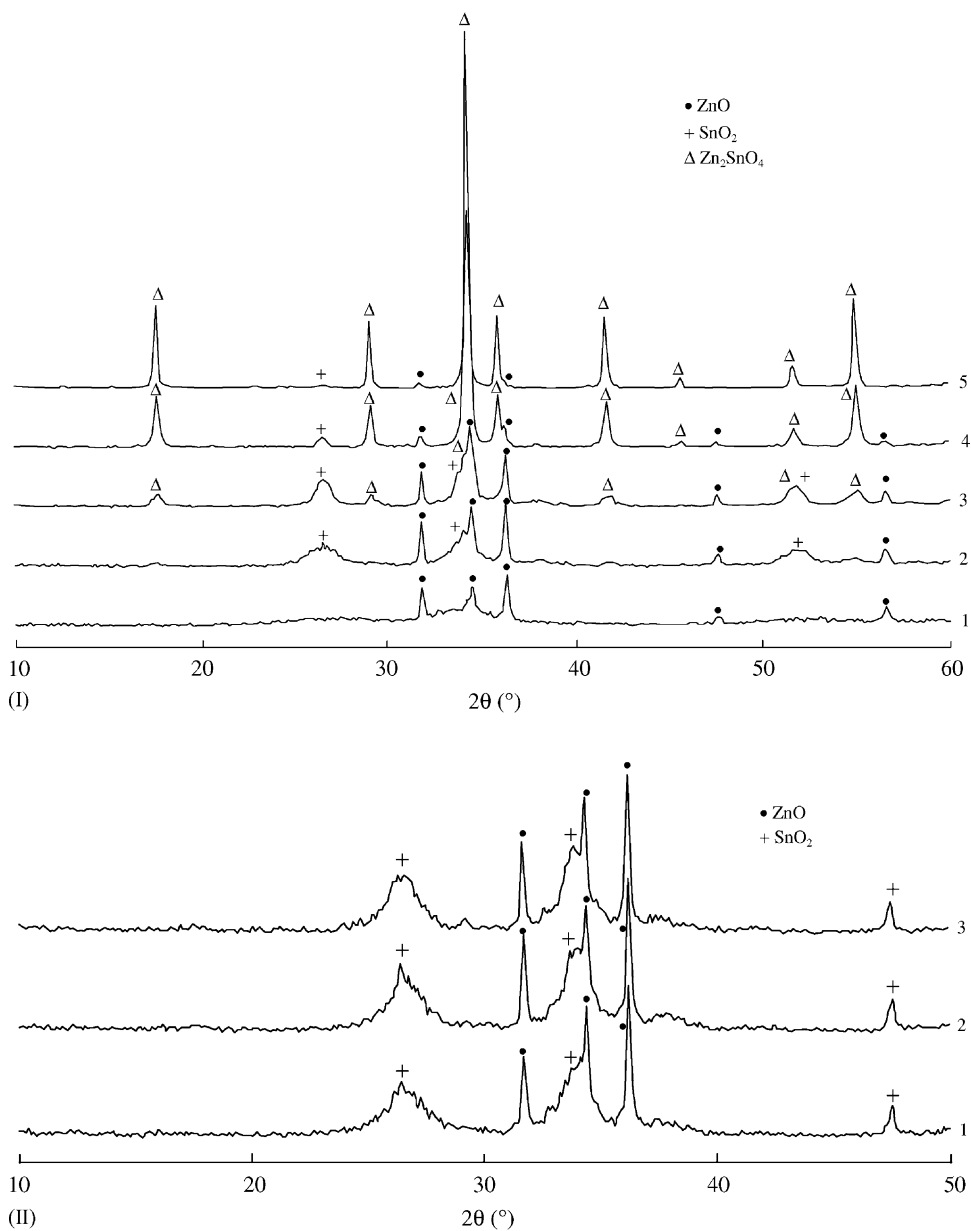| Heat-treating conditions (°C)						
500	600			700	800	900
Time (h)						
10	2	6	10	10	10	10
Phase/mean size (nm)						
ZnO/31.0	ZnO/39.3	ZnO/42.6	ZnO/46.4	ZnO/97.9	ZnO (a little)	ZnO (little)
SnO_2/amorphous	SnO_2/2	SnO_2/2.7	SnO_2/3.9	SnO_2/8.2	SnO_2 (a little)	SnO_2 (little)
				Zn_2SnO_4/15.4	Zn_2SnO_4/45.4	Zn_2SnO_4/166.5

Fig. 1. (1) The XRD patterns of Z_2S calcined at different temperatures for 10 h. (1) 500 °C; (2) 600 °C; (3) 700 °C; (4) 800 °C; (5) 900 °C. (2) The XRD patterns of Z_2S calcined at 600 °C for different times. (1) 2 h; (2) 6 h; (3) 10 h.

that the mean sizes of ZnO and SnO_2 in Z_2S are significantly less than that of pure ZnO and SnO_2 calcined at the same condition, respectively. For ZnO, the present result is in agreement with the literature results that larger additions of SnO_2 cause a decrease in the mean grain size of ZnO [25,26]. The mean size of SnO_2 in ZS is less than that of pure SnO_2 but larger than that of SnO_2 in Z_2S under the identical heat-treating condition, meaning that doping ZnO restrains SnO_2 from crystal growth, which is similar to the result of the

Table 2
Relationship between BET and calcination temperature

Calcination temperature (°C)[a]	BET (m^2/g)			
	Z_2S	ZS	ZnO	SnO_2
600	30.95	20.13	6.25	20.89
700	20.48			
800	4.02			
900	2.15			

[a] All samples were calcined for 10 h.

In$_2$O$_3$-doped SnO$_2$ [27]. But it also reported that doping ZnO in small amounts (e.g. 3 mol.% or 3 wt.% of ZnO) shows little effect on the particle size of SnO$_2$ [28,29].

3.2. Effect of calcination temperature on specific surface area (BET)

The BET of Z_2S calcined at different temperatures are listed in Table 2. For comparison, the BET of ZS, SnO$_2$ and ZnO are also listed in Table 2. Comparing Table 2 with Table 1, it can be seen that the BET is closely related to the mean size of the sample particles. The larger the mean size, the less is the BET. The BET is decreased as the calcination temperature increases. From Table 2, BET is found to be in the order of Z_2S > ZS > ZnO, indicating that the addition of SnO$_2$ prevents the densification and the growth of ZnO grains and consequently results in more porous microstructure than pure ZnO [26].

3.3. Adsorption behavior of Z_2S

MO can be adsorbed onto Z_2S from its aqueous solution. A measurable decrease in the concentration of the MO solution was observed upon equilibrating it overnight with Z_2S powders in the dark:

$$MO + Z_2S \rightleftharpoons MO \cdots Z_2S$$
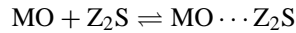
The isothermal adsorption curve of MO on Z_2S is illustrated in Fig. 2. Obviously, the isothermal adsorption process is a two-stage process that is neither similar to the adsorption of acid orange 7 on TiO$_2$ [30], a process fitted by Langmuir equation, nor similar to that of reactive brilliant red K-2G, reactive yellow KD-3G, acid red B, cationic pink FG and cationic blue X-GRL, respectively, on the surface bond-conjugated TiO$_2$/SiO$_2$, a process fitted by Freundlich equation [31]. Under the low equilibrium concentration of MO, the first adsorption equilibrium can be reached at the MO
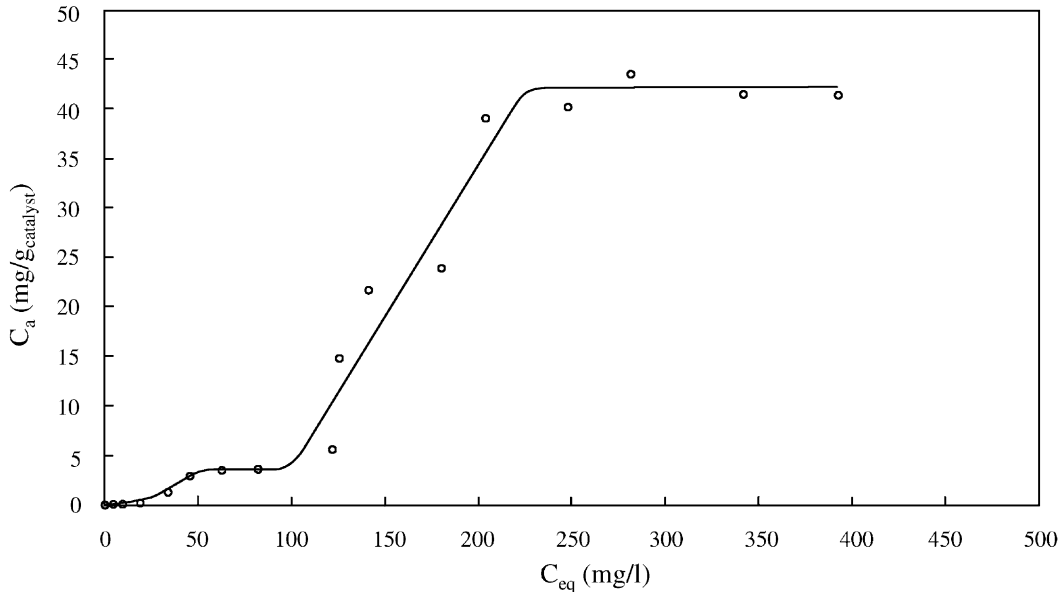

Fig. 2. The adsorption isotherm of MO on Z_2S calcined at 600 °C for 2 h as a function of the equilibrium concentration of MO: temperature, 25 ± 2 °C; Z_2S, 5 g/l.
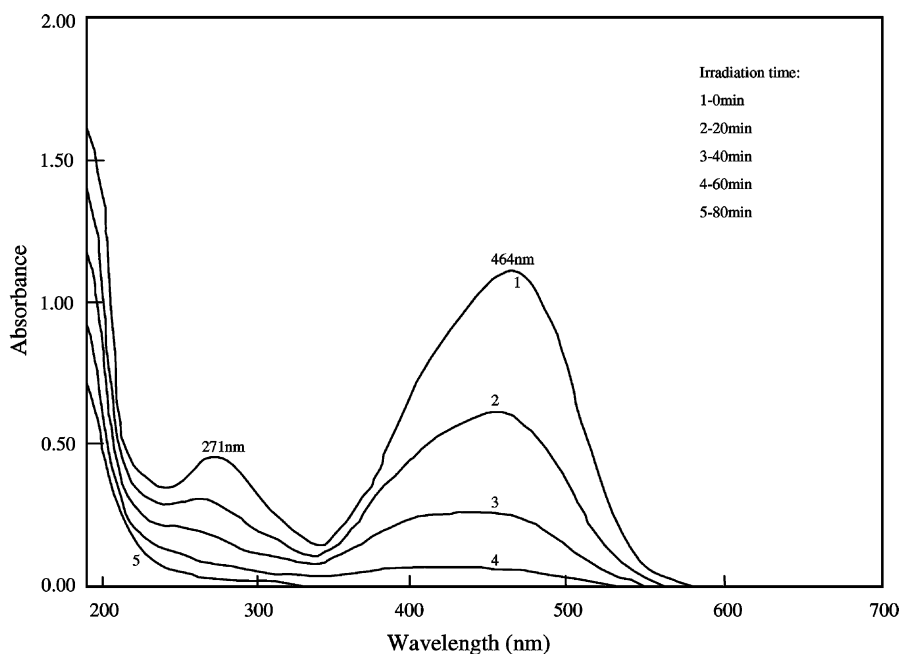
Fig. 3. Absorbance spectral changes of MO solution after different irradiation times in the presence of Z_2S calcined at 600 °C for 2 h: Z_2S, 2.5 g/l; MO, 20 mg/l.

equilibrium concentration (C_{eq}) of about 58.7 mg/l corresponding to the saturation adsorption (C_a) of about 3.5 mg/$g_{catalyst}$. With the C_{eq} increases, the second saturation adsorption of about 42.2 mg/$g_{catalyst}$ can be reached at $C_{eq} \approx 230$ mg/l. The two-stage adsorption process may relate to the double compositions of ZnO and SnO_2 in Z_2S with different affinity to MO and the adsorption isotherm of MO on Z_2S may be a combination of possibly Langmuir adsorption of MO on ZnO and that on SnO_2 in Z_2S. An explanation of this adsorption mechanism is under further study.

3.4. Photocatalytic activity of the photocatalysts

3.4.1. Degradation kinetics of MO

The time-dependent UV–VIS spectra of MO during the irradiation are illustrated in Fig. 3. It can be seen that the maximum absorbance of 464 nm disappears completely after irradiation for about 80 min. The degradation rate of MO on Z_2S is as shown in Fig. 4. A blank experiment in the absence of irradiation but with Z_2S demonstrates that no MO degradation occurs. Another blank experiment in the absence of Z_2S but under irradiation shows that MO cannot

be degraded under the present experimental condition. The results of the blank experiments are as shown in Fig. 4.

For the purposes of comparison, the experiments of degrading MO photocatalytically using ZS, pure
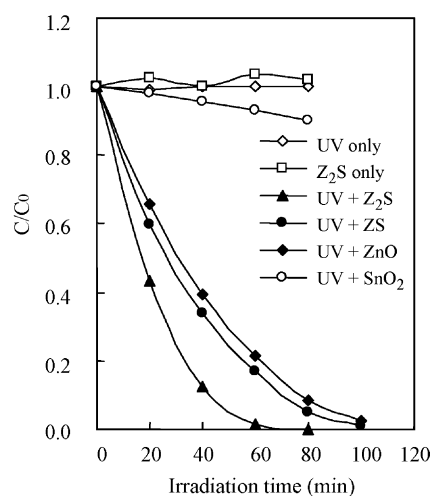

Fig. 4. The photocatalytic activity of photocatalysts calcined at 600 °C for 10 h: photocatalysts, 2.5 g/l; MO, 20 mg/l.

Table 3
Degradation rate constants of MO using different photocatalysts

Photocatalyst[a]	Rate constant (k)[b] (mg/l min)	Ratio of rate constant
Z_2S	0.5657 (k_1)	–
ZS	0.4036 (k_2)	1.402 (k_1/k_2)
ZnO	0.3406 (k_3)	1.661 (k_1/k_3)
SnO_2	0.0215 (k_4)	26.31 (k_1/k_4)

[a] All photocatalysts were calcined at 600 °C for 10 h.
[b] Calculated by considering the first 20 min of irradiation.

SnO_2 and pure ZnO, respectively, have been done. The results are also as shown in Fig. 4. It can be seen that Z_2S is a more effective photocatalyst to MO than ZS and ZnO and SnO_2 shows a little photocatalytic activity, which agrees with the literature result [11]. The rate constants of degrading MO using Z_2S, ZS, ZnO and SnO_2 as photocatalysts are listed in Table 3.

The degradation rate of MO using Z_2S as photocatalyst is faster than that using ZS, ZnO and SnO_2 as photocatalyst by 40.2, 66.1 and 2531%, respectively.

3.4.2. Total organic carbon elimination

The TOC elimination curve of MO is as shown in Fig. 5. It is worth noting that 38.9% of TOC still remain after the decolorization process is completed. Moreover, the mineralization rate became very slow

after irradiation of 140 min, indicating the formation of some long-lived by-products, which have low rate constants of reactions with hydroxyl radicals [32,33]. Indeed, even an extended irradiation of over 200 min does not induce a complete conversion of the organic materials to water, carbon dioxide and other inorganic species and about 18.9% of TOC remain.

Despite of difficulty to get MO mineralized completely, the long-lived by-products are generally less harmful or harmless to environment and can be further treated by biological methods [34]. So, Z_2S may be applied to photocatalytically treating some persistent organic pollutants.

3.4.3. Effect of heat-treatment for photocatalyst on the photocatalytic activity

The effect of heat-treating temperature on the photocatalytic activity of Z_2S is as shown in Fig. 6. It can be seen that the degradation rate of MO is decreased with the increasing calcination temperature of Z_2S. The photocatalytic activity of Z_2S is significantly reduced at higher calcination temperature (900 °C), but the photocatalytic activity of Z_2S has no significant difference among the photocatalysts calcined at 600, 700 and 800 °C, respectively. The significant decrease in the photocatalytic activity of Z_2S calcined at 900 °C compared with that of Z_2S calcined at 800 °C may be
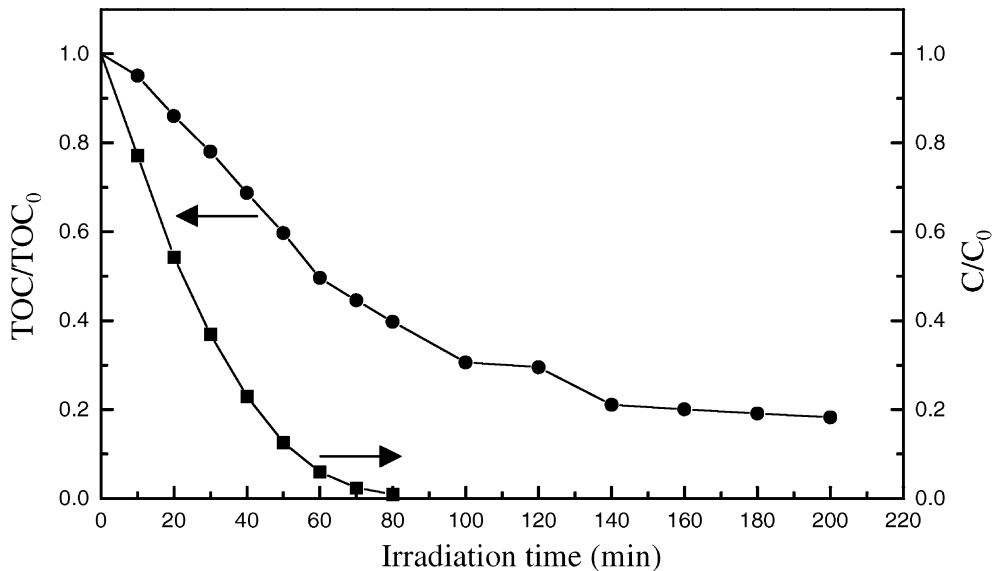

Fig. 5. The TOC elimination kinetics of MO photocatalytic degradation by Z_2S calcined at 600 °C for 2 h: Z_2S, 2.5 g/l; MO, 20 mg/l.
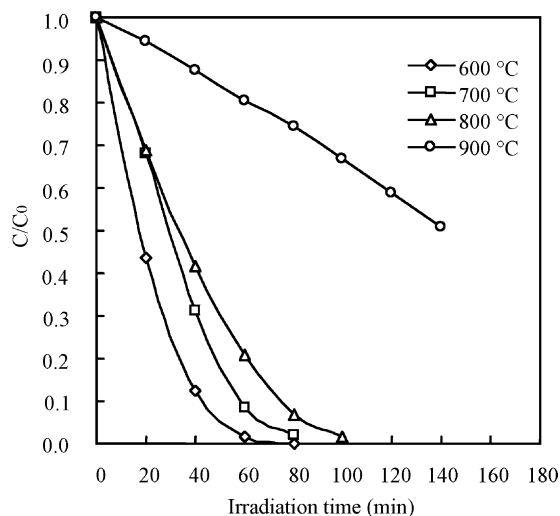
Fig. 6. The effect of calcination temperature (for 10 h) on the photocatalytic activity of Z_2S: Z_2S, 2.5 g/l; MO, 20 mg/l.

Fig. 7. The effect of pH on the photocatalytic activity of Z_2S calcined at 600 °C for 2 h: Z_2S, 2.5 g/l; MO, 20 mg/l.

attributed to the variation in phase composition and in particle size with the increasing calcination temperature. As mentioned previously, Z_2S calcined at 600 °C consists only of ZnO and SnO_2 and no Zn_2SnO_4 phase is found. Zn_2SnO_4 emerges at 700 °C and Zn_2SnO_4, which exhibits poorer photocatalytic activity comparatively [35], is almost the only phase when calcined at 900 °C. Moreover, higher calcination temperature causes the growth of particles, which is supported by XRD, leading to the decrease in BET, therefore, resulting in the decrease in photocatalytic activity [36,37].

3.4.4. Effect of pH on the photocatalytic activity

The heterogeneous photocatalysis has been found to be pH dependent [38–42]. As an amphoteric oxide, ZnO is chemically stable in the pH range of $4 \leq pH \leq 14$ [40,43], otherwise will be dissolved. So, the experiments about the effect of pH on the photodegradation rate of MO were done at the pH = 4.22, 7.12 (natural) and 12.57. The results are depicted in Fig. 7. At low pH, the positively charged Z_2S offers a suitable surface for adsorption of MO anion [41]. Increasing the pH reduces adsorption and gradually increases the electrostatic repulsion between the MO anion ($pK_1 = 3.46$) and the oxide surface. The drastic decrease in degradation rate can be seen at pH = 12.57, which is probably due to the coulombic repulsion between the anions and the highly nega-
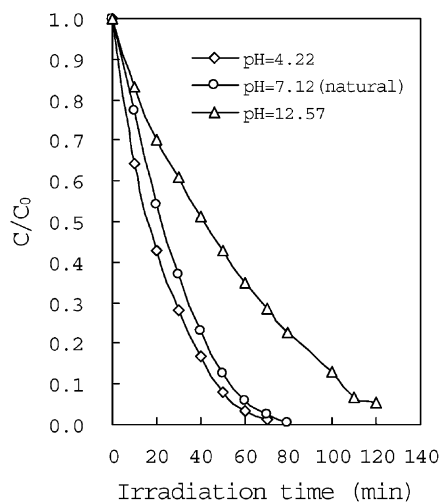
tive charged oxide surface and degradation would, thus, depend on diffusion of surface-generated OH$^\bullet$ towards the double layer to the low concentration of MO anion, a slower process than direct charge transfer [41]. Additionally, the increase of pH might cause a cathodic displacement of the valence band position of ZnO and SnO_2 in the Z_2S, which results in the weakening of the oxidation ability of the holes [41].

3.5. Effect of electrolytes on the photocatalytic activity

Inorganic ions may be specific adsorption or alternative forms at the surface of photocatalyst, thus, they can affect the photocatalytic oxidation. Some studies [44–49] have systematically investigated the influences of anions, such as SO_4^{2-}, NO_3^-, Cl^-, ClO_4^- and CO_3^{2-}, on the photocatalytic activity of TiO_2 towards certain organic substrates. Fig. 8 shows the changes of the ratios of the residual MO concentrations to its initial ones with time, illustrating the effect of Cl^-, NO_3^- and SO_4^{2-} on the photocatalytic degradation of MO under the natural pH (7.12). NaCl shows inhibitive effect on the reaction and the influence is enhanced with the increasing NaCl concentration. Cl^- is regarded as a radical scavenger that may retard the photocatalytic oxidation reaction dramatically [47,49]. NO_3^- shows little
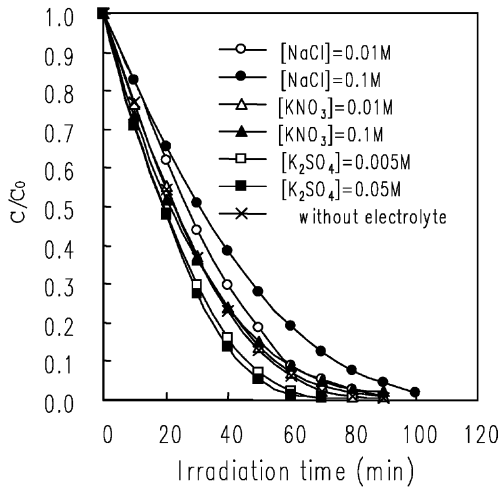
Fig. 8. The effect of electrolytes on the photocatalytic activity of Z_2S calcined at 600 °C for 2 h: Z_2S, 2.5 g/l; MO, 20 mg/l.

effect on the photocatalytic activity, which agrees with the literature results [45,46]. The reactions were promoted by SO_4^{2-} and the promotion is enhanced with SO_4^{2-} concentration. The sulfate might react with $OH^\bullet$ radical to produce sulfate radical [45,49]:

$$SO_4^{2-} + OH^\bullet \rightarrow SO_4^{\bullet 2-} + H_2O$$
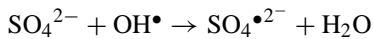
As a stronger oxidizing agent, the sulfate radical could accelerate the photocatalytic reaction.

3.6. The mechanism of photocatalytic activity of MO on Z_2S and ZS

The UV–VIS diffuse reflectance spectrum of Z_2S is as shown in Fig. 9 [50–52]. For comparison, the UV–VIS diffuse reflectance spectra of ZS, ZnO and SnO_2 are also presented. The band gap absorption edge of Z_2S is determined to be 394 nm [53–55], corresponding to the band gap energy of 3.15 eV [56]. The band gap absorption edge of ZS, ZnO and SnO_2 are determined to be 397, 391 and 490 nm corresponding to the band gap energy to be 3.12, 3.17 and 2.53 eV, respectively. The band gap absorption edges and the band gap energies are listed in Table 4.

The experimental result for the band gap energy of ZnO is in reasonable agreement with the accepted literature value of 3.2 eV [56]. But for SnO_2, the band gap energy value is 2.53 eV, which is significantly
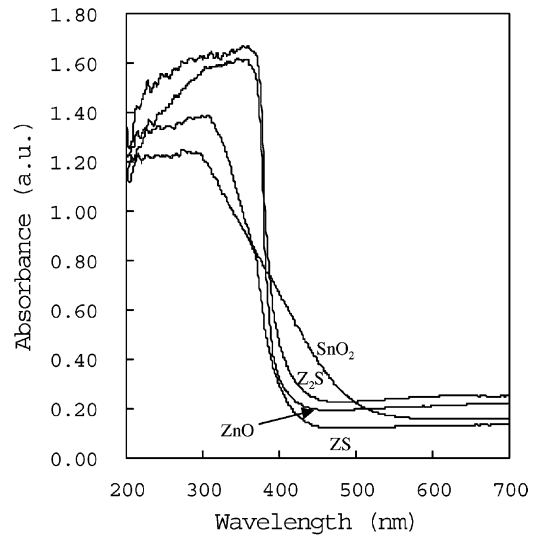

Fig. 9. The UV–VIS diffuse reflectance spectra of Z_2S, ZS, ZnO and SnO_2 samples calcined at 600 °C for 10 h.

less than the literature value of 3.8 eV [56]. A similar result was reported in [57]. The reason for this phenomenon could probably be attributed to the imperfect crystallization of SnO_2. As mentioned above, under the heat-treating condition of 600 °C for 10 h, Z_2S is composed of ZnO and SnO_2 and ZS is composed of Zn_2SnO_4 and SnO_2. From Table 4, it can be seen that the band gap energy of Z_2S is neither that of ZnO nor of SnO_2. Similarly the band gap energy of ZS is neither that of Zn_2SnO_4 (3.4 eV) [58] nor of SnO_2.

Referring to the previous papers [6,10,59], a mechanistic scheme of the charge separation and the photocatalytic activity for the photocatalysts is as shown in Fig. 10.

ZnO can be excited by the photons with the wavelengths under 391 nm and produces the photogenerated electron/hole pairs, showing photocatalytic

Table 4
Absorption edges and band gap energies of Z_2S, ZS, ZnO and SnO_2

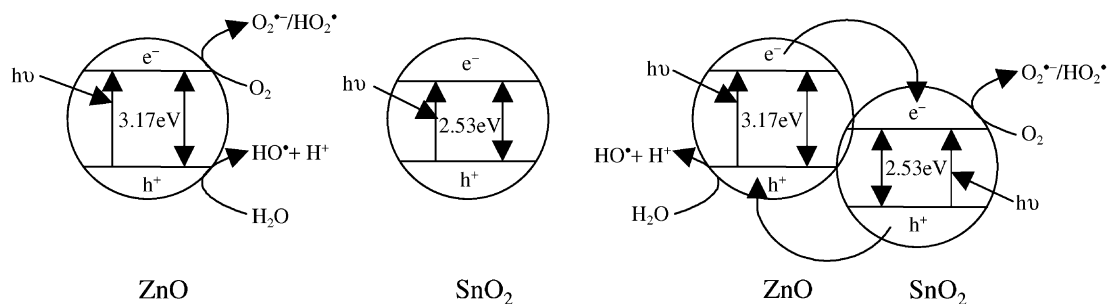| Sample[a]	Absorption edge (nm)	Band gap energy (eV)
Z_2S	394	3.15
ZS	397	3.12
ZnO	391	3.17
SnO_2	490	2.53

[a] All samples were calcined at 600 °C for 10 h.

Fig. 10. A schematic diagram illustrating the principle of charge separation and photocatalytic activity for the photocatalysts.

activity. For SnO_2 with the band gap energy of 2.53 eV, theoretically it can be excited by the photons with the wavelengths under 490 nm, but it shows only a little photocatalytic activity under UV light in the present experimental conditions. This is probably due to the fast recombination of the photogenerated electron/hole pairs in SnO_2. Z_2S with the band gap energy of 3.15 eV, can be excited by the photons with the wavelengths under 394 nm. The CB of SnO_2 is lower than that of ZnO so that the former can act as a sink for the photogenerated electrons [6,10,56]. Since, the holes move in the opposite direction from the electrons, photogenerated holes might be trapped within the ZnO particle, making charge separation more efficient, resulting in Z_2S shows stronger photocatalytic activity [10]. Compared to ZnO, Zn_2SnO_4 shows lower photocatalytic activity and SnO_2 has a little photocatalytic activity, but ZS coupled oxide photocatalyst shows even higher photocatalytic activity than that of ZnO. The reason may be that, in addition to the larger BET of ZS than ZnO, which is in favor of high photocatalytic activity, in the ZS coupled photocatalyst, the recombination of the photogenerated electron/hole pairs is suppressed and, therefore, resulting in ZS exhibits higher photocatalytic activity.

4. Conclusions

1. The nano-sized photocatalysts Z_2S and ZS can be synthesized by using the co-precipitation method. With the increase in calcination temperature, not only the mean grain sizes of Z_2S grow, but also the change in phase of the photocatalyst occurs.

2. Z_2S exhibits better photocatalytic activity to MO than ZS and ZnO. The photocatalytic reaction by Z_2S is 40.2 and 66.1% faster than those by ZS and ZnO, respectively. A mechanistic scheme for photocatalytic activity is presented to explain the experimental results. The heat-treating condition for photocatalyst, pH and electrolytes, such as NaCl, KNO_3 and K_2SO_4, are among the factors affecting the photocatalytic activity.

Acknowledgements

References

[1] M.R. Hoffmann, S.T. Martin, W.Y. Choi, D.W. Bahnemann, Chem. Rev. 95 (1995) 69.
[2] P. Qu, J.C. Zhao, T. Shen, H. Hidaka, J. Mol. Catal. Part A. Chem. 129 (1998) 257.
[3] P. Peralta-Zamora, S.G. de Moraes, R. Pelegrini, M. Freire Jr., J. Reyes, H. Mansilla, N. Duran, Chemosphere 36 (1998) 2119.
[4] A.L. Linsebigler, G.Q. Lu, J.T. Yates Jr., Chem. Rev. 95 (1995) 735.

[5] T. Torimoto, S. Ito, S. Kuwabata, H. Yoneyama, Environ. Sci. Technol. 30 (1996) 1275.

[6] K. Tennakone, J. Bandara, Appl. Catal. Part A. Gen. 208 (2001) 335.

[7] I. Bedja, P.V. Kamat, J. Phys. Chem. 99 (1995) 9182.

[8] K. Vinodgopal, I. Bedja, P.V. Kamat, Chem. Mater. 8 (1996) 2180.

[9] J. Lin, J.C. Yu, D. Lo, S.K. Lam, J. Catal. 183 (1999) 368.

[10] K. Vinodgopal, P.V. Kamat, Environ. Sci. Technol. 29 (1995) 841.

[11] L.Y. Shi, C.Z. Li, H.C. Gu, D.Y. Fang, Mater. Chem. Phys. 62 (2000) 62.

[12] K.Y. Song, M.K. Park, Y.T. Kwon, H.W. Lee, W.J. Chung, W.I. Lee, Chem. Mater. 13 (2001) 2349.

[13] T. Ohno, F. Tanigawa, K. Fujihara, S. Izumi, M. Matsumura, J. Photochem. Photobiol. Part A. Chem. 118 (1998) 41.

[14] Y.R. Do, W. Lee, K. Dwight, A. Wold, J. Solid State Chem. 108 (1994) 198.

[15] Y.T. Kwon, K.Y. Song, W.I. Lee, G.J. Choi, Y.R. Do, J. Catal. 191 (2000) 192.

[16] X.Z. Li, F.B. Li, C.L. Yang, W.K. Ge, J. Photochem. Photobiol. Part A. Chem. 141 (2001) 209.

[17] B. Pal, M. Sharon, G. Nogami, Mater. Chem. Phys. 59 (1999) 254.

[18] B. Pal, T. Hata, K. Goto, G. Nogami, J. Mol. Catal. Part A. Chem. 169 (2001) 147.

[19] J.C. Yu, J. Lin, R.W.M. Kwok, J. Phys. Chem. B 102 (1998) 5094.

[20] Y.Q. Wang, H.M. Cheng, L. Zhang, Y.Z. Hao, J.M. Ma, B. Xu, W.H. Li, J. Mol. Catal. Part A. Chem. 151 (2000) 205.

[21] J. Lin, J.C. Yu, J. Photochem. Photobiol. Part A. Chem. 116 (1998) 63.

[22] S.P. Ruan, F.Q. Wu, T. Zhang, W. Gao, B.K. Xu, M.Y. Zhao, Mater. Chem. Phys. 69 (2001) 7.

[23] H.P. Klug, L.E. Alexander, X-Ray Diffraction Procedures for Polycrystalline and Amorphous Materials, Wiley, New York, 1974, p. 618.

[24] J.H. Yu, G.M. Choi, Sens. Actuators B 61 (1999) 59.

[25] N. Daneu, A. Recnik, S. Bernik, D. Kolar, J. Am. Ceram. Soc. 83 (2000) 3165.

[26] J.H. Yu, G.M. Choi, Sens. Actuators B 52 (1998) 251.

[27] H. Yang, S.D. Han, L. Wang, I.J. Kim, Y.M. Son, Mater. Chem. Phys. 56 (1998) 153.

[28] J.H. Yu, G.M. Choi, Sens. Actuators B 75 (2001) 56.

[29] T. Kimura, S. Inada, T. Yamaguchi, J. Mater. Sci. 24 (1989) 220.

[30] K. Vinodgopal, D.E. Wynkoop, P.V. Kamat, Environ. Sci. Technol. 30 (1996) 1660.

[31] C. Hu, Y.Z. Wang, H.X. Tang, Appl. Catal. Part B. Environ. 35 (2001) 95.

[32] N.K.V. Leitner, M. Dore, J. Photochem. Photobiol. Part A. Chem. 99 (1996) 137.

[33] C. Galindo, P. Jacques, A. Kalt, J. Photochem. Photobiol. Part A. Chem. 130 (2000) 35.

[34] C. Hu, Y.Z. Wang, Chemosphere 39 (1999) 2107.

[35] C. Wang, X.M. Wang, J.C. Zhao, B.X. Mai, G.Y. Sheng, P.A. Peng, J.M. Fu, J. Mater. Sci. 37 (2002) 1.

[36] A. Towata, Y. Uwamino, M. Sando, K. Iseda, H. Taoda, NanoStruct. Mater. 10 (1998) 1033.

[37] L.G. Devi, G.M. Krishnaiah, J. Photochem. Photobiol. Part A. Chem. 121 (1999) 141.

[38] M.S.T. Goncalves, A.M.F. Oliveira-campos, E.M.M.S. Pinto, P.M.S. Plasencia, M.J.R.P. Queiroz, Chemosphere 39 (1999) 781.

[39] J. Bangun, A.A. Adesina, Appl. Catal. Part A. Gen. 175 (1998) 221.

[40] A.A. Khodja, T. Sehili, J.F. Pilichowski, P. Boule, J. Photochem. Photobiol. Part A. Chem. 141 (2001) 231.

[41] I. Poulios, M. Kositzi, A. Kouras, J. Photochem. Photobiol. Part A. Chem. 115 (1998) 175.

[42] F. Kiriakidou, D.I. Kondarides, X.E. Verykios, Catal. Today 54 (1999) 119.

[43] D.E. Scaife, Solar Energy 25 (1980) 41.

[44] D.W. Chen, A.K. Ray, Water Res. 32 (1998) 3223.

[45] K.H. Wang, Y.H. Hsieh, M.Y. Chou, C.Y. Chang, Appl. Catal. Part B. Environ. 21 (1999) 1.

[46] W.H. Leng, H. Liu, S.A. Cheng, J.Q. Zhang, C.N. Chao, J. Photochem. Photobiol. Part A. Chem. 131 (2000) 125.

[47] I. Arslan, I.A. Balcioglu, D.W. Bahnemann, Appl. Catal. Part B. Environ. 26 (2000) 193.

[48] A. Piscopo, D. Robert, J.V. Weber, Appl. Catal. Part B. Environ. 35 (2001) 117.

[49] M. Abdullah, G.K.-C. Low, R.W. Matthews, J. Phys. Chem. 94 (1990) 6820.

[50] H. Yamashita, S. Kawasaki, Y. Ichihashi, M. Harada, M. Takeuchi, M. Anpo, G. Stewart, M.A. Fox, C. Louis, M. Che, J. Phys. Chem. B 102 (1998) 5870.

[51] Q.H. Zhang, L. Gao, J.K. Guo, Appl. Catal. Part B. Environ. 26 (2000) 207.

[52] D. Dvoranova, V. Brezova, M. Mazur, M.A. Malati, Appl. Catal. Part B. Environ. 37 (2002) 91.

[53] P.L. Provenzano, G.R. Jindal, J.R. Sweet, W.B. White, J. Luminesc. 92 (2001) 297.

[54] J.H. Park, P.M. Woodward, Int. J. Inorg. Mater. 2 (2000) 153.

[55] K.H. Chung, D.C. Park, J. Mol. Catal. Part A. Chem. 129 (1998) 53.

[56] A. Hagfeldt, M. Gratzel, Chem. Rev. 95 (1995) 49.

[57] Y. Yamashita, K. Yoshida, M. Kakihana, S. Uchida, T. Sato, Chem. Mater. 11 (1999) 61.

[58] Z.Y. Chen, Y. Jia, Z.D. Zhang, Y.T. Qian, J. Univ. Sci. Technol. China 17 (1987) 343 (in Chinese).

[59] D. Beydoun, R. Amal, G.K.-C. Low, S. McEvoy, J. Phys. Chem. B 104 (2000) 4387.